Numerical Investigation of Stress and Strain Nonuniformities in Direct Simple Shear Sample and Its Effects on Overall Stress–Strain Behaviour

Sudipta Bhowmick & Bipul Hawlader
Department of Civil Engineering, Memorial University of Newfoundland, St. John's, Newfoundland and Labrador, Canada

GeoCalgary 2022 October 2-5 Reflection on Resources

ABSTRACT
The stress state in many geotechnical problems is similar to the simple shear conditions. While direct shear and triaxial tests are commonly performed for practical engineering and research activities, the direct simple shear (DSS) test facilities are available in some advanced laboratories. One of the limitations of the DSS test is that only the vertical normal and horizontal shear stresses are measured in most cases. The unknown shear stress on the vertical boundary makes the interpretation of the test results difficult. In addition, stress and strain nonuniformities might occur in the sample. In the present study, three-dimensional finite element (FE) modelling of stacked-ring type DSS samples is performed for different soil conditions to investigate the possible nonuniformities and their effects on the interpreted strength parameters. The FE simulated results are compared with the laboratory test results on sand. The applicability and limitations of DSS tests are highlighted.

RÉSUMÉ
L'état de contrainte dans de nombreux problèmes géotechniques est similaire aux conditions de cisaillement simples. Alors que les tests de cisaillement direct et triaxiaux sont couramment effectués pour les activités pratiques d'ingénierie et de recherche, les installations de test de cisaillement simple direct (DSS) sont disponibles dans certains laboratoires avancés. L'une des limites du test DSS est que seules les contraintes de cisaillement normales verticales et horizontales sont mesurées dans la plupart des cas. La contrainte de cisaillement inconnue sur la limite verticale rend difficile l'interprétation des résultats des essais. De plus, des non-uniformités de contrainte et de déformation peuvent se produire dans l'échantillon. Dans la présente étude, une modélisation tridimensionnelle par éléments finis (EF) d'un échantillon DSS de type anneau empilé est réalisée pour différentes conditions de sol afin d'étudier les non-uniformités possibles et leurs effets sur les paramètres de résistance interprétés. Les résultats simulés par EF sont comparés aux résultats des essais en laboratoire sur sable. L'applicabilité et les limites des tests DSS sont mises en évidence.

1 INTRODUCTION

In geotechnical laboratories, several devices are used to determine the shear strength parameters of soil, including commonly used direct shear (DS) and triaxial (TX) tests apparatus. Advanced systems, such as direct simple shear (DSS), plane strain, and hollow cylinder torsional shear test apparatus, were also developed to apply complex loadings that better represent the field behaviour. The simple shear condition is a loading condition that better represents many field conditions, such as slope failure along a riverbank or embankment, pipeline–soil and pile–soil interactions.

For simple shear loading, direct simple shear device and hollow cylinder torsional apparatus (HCA) are generally used. While a better measurement and control of the stresses can be performed in the HCA, the sample preparation is relatively difficult and time consuming. On the other hand, sample preparation and DSS testing are relatively simple (Bernhardt et al. 2016). Over the last few decades, a variety of DSS devices were developed (e.g., NGI type and Cambridge type). Among them, the NGI-type is the commonly used DSS apparatus that uses the cylindrical specimen with a wire-reinforced membrane to provide the lateral confinement. In recent years, stacked rings instead of a wire-reinforced membrane are used.

Several researchers discussed the advantages and disadvantages of these DSS devices (Frydman and Talesnick 1991; Shibuya and Hight 1987). One of the major advantages of DSS is that it allows the rotation of the principal stresses during shearing, which cannot be done in a triaxial test. One of the main limitations of DSS testing is the missing information on the shear and normal stresses on the vertical plane in a typical DSS apparatus, which makes the interpretation of test results difficult. However, many researchers agreed that the core part of the soil specimen is in simple shear condition, and the nonuniformity occurs mainly near the boundary. Unfortunately, no consensus has been reached and a varying degree of nonuniformity was reported.

Measurement of stress and strain nonuniformities within the sample is difficult, if not impossible. Therefore, numerical simulations could be an alternative to understand further insights into the mechanisms and overall response. Some studies used Discrete Element Methods (DEM) to simulate DSS tests (Asadzadeh and Soroush 2016; Bernhardt et al. 2016; Dabeet et al. 2015; Guo et al. 2022). While it provides some valuable information, one of the limitations of DEM is the defining some input parameters, such as interparticle frictional resistance. Finite element methods have also been used to simulate DSS tests (Doherty and Fahey 2011, Potts et al.

1987; Wai et al. 2021; Wu 2017). Wai et al. (2021) simulated monotonic DSS tests only for limited strain (< 4%), and therefore the behaviour of soil for a wider range of strains was not investigated.

The objective of the present study is to understand the behaviour of soil elements in a DSS soil specimen and the effects of nonuniformity on the overall response by conducting FE simulations.

2 FINITE ELEMENT MODELING

Three-dimensional FE analysis is performed using Abaqus/Explicit FE software (Dassault Systemes 2019). A circular soil specimen of diameter D = 70 mm, height H = 20 mm is sheared up to 20% shear strain. Taking advantage of symmetry, only half of the specimen is modelled. Figure 1 shows the typical FE mesh used in the present study. A structured mesh is created by zoning the soil. An adaptive mesh domain with Lagrangian type boundary regions is used to improve the aspect ratio of the elements.

The top cap and bottom pedestal are modelled by 2-mm thick rigid plates. Twenty-two rigid stacked rings of an internal diameter of 70 mm, a width of 2 mm and a thickness of 1 mm (each) are used to provide lateral restraint. The diameter of the top plate is 70 mm, which is the same as the internal diameter of the stacked rings and the diameter of the soil sample such that the top plate can move vertically during loading. The diameter of the bottom plate is 74 mm (i.e., same as the outer diameter of the stacked ring). Mesh convergence analysis has been performed for this study. The detailed analysis shown in this paper has an approximate element size of 0.5 mm, and the total number of elements for the analysis was 80949. Analysis has also been performed with finer mesh density, but no significant difference was found in those analysis results.

The soil in the specimen is discretized by Lagrangian eight-node linear brick elements having reduced integration and hourglass control. The interface between the soil and the inner surface of the stacked rings is frictionless. Abaqus general contact algorithm is used to model this frictionless contact behaviour. To prevent sliding, rigid frictional interface conditions are used for the interfaces between soil and the top and bottom plates. Also, the top and bottom plates are not allowed to rotate during loading.

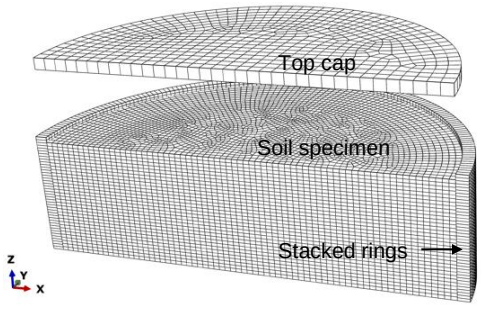

Figure 1. Typical finite element mesh prior to loading

Each simulation is performed in two steps. In the first step, the specimen is consolidated under K_0 condition by applying vertical load on the top plate. As the simulations are performed for dry sand, the term consolidation in this paper represents vertical one-dimensional compression without modelling pore pressure dissipation. In the shearing stage, keeping the top plate fixed to horizontal movements, the bottom plate is displaced leftward along the x-direction (Fig. 1) at a rate of 0.004 m/s without rotation and vertical displacement. The vertical displacement of the top plate provides the volume change of the specimen. The method of simulation described above represents the conditions similar to those used in laboratory tests by Al Tarhouni and Hawlader (2021).

Simulations are performed for constant normal stress (σ_z') conditions. That means, a given σ_z' is applied in the consolidation stage, and σ_z' remains constant in the shearing stage. Analyses are performed for medium dense dry sand. The parameters used in numerical simulations are listed in Table 1. The soil is modelled as linear elastic perfectly plastic material using the Mohr–Coulomb model. The authors understand that some level of strain-softening would occur in medium dense sand; however, it has not been modelled in the present study. In other words, the simulations are performed for the constant angle of internal friction (ϕ') and dilation angle (ψ).

Table 1. Dimensions and geotechnical parameters used in FE analysis

Parameters	Values
Diameter of soil specimen, D (mm)	70
Height of soil specimen, H (mm)	20
Young's modulus of soil, E (MPa)	10
Poisson's ratio of soil, ν_{soil}	0.3
Angle of internal friction of soil, ϕ' (°)	38
Dilation angle of soil, ψ (°)	8
Unit weight of soil, γ_{soil} (kN/m^3)	16.9

3 RESULTS

3.1 Stress–strain behaviour

Figure 2(a) shows the simulated stress–strain behaviour for σ_z' = 50, 100, and 200 kPa. Figure 2(b) shows the variation of stress ratio R (= τ_{zx}/σ_z') with shearing. A similar stress–strain behaviour was found from DSS tests on silica sand for similar test conditions (Al Tarhouni and Hawlader 2021).

Young's modulus (E) of sand increases with confining pressure (Hardin and Black 1966). However, a stress-independent constant value of E is used in this study. Figure 2(a) shows that, at the early stage of shearing, τ_{zx} increases linearly with shear strain, which is almost independent of confining pressure. However, when the simulation results are plotted in terms of stress ratio (Fig. 2(b)), it shows that R increases at a slower rate for higher σ_z'. Note that all the elements do not reach the same stress ratio for a given applied shear strain (γ) at the

boundary, rather the failure occurs progressively, which could cause different level of nonuniformity for varying σ_z'. Therefore, R vs γ curves are not the same for all σ_z', although the same value of ϕ' and ψ are used.

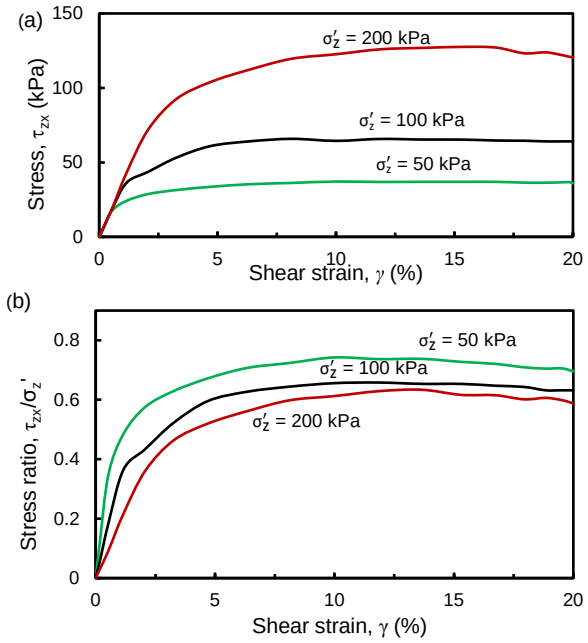

Figure 2. Finite element simulation results: (a) stress-strain response; (b) variation of stress ratio

4 ESTIMATION OF STRESSES TO CONSTRUCT MOHR'S CIRCLE

Based on the measurements in a typical DSS tests, the following stress and strain components can be calculated: vertical normal stress (σ_z'), shear stress (τ_{zx}), axial strain (ε_z) and shear strain (γ_{zx}). The location of σ_z' and τ_{zx} is shown in Fig. 3.

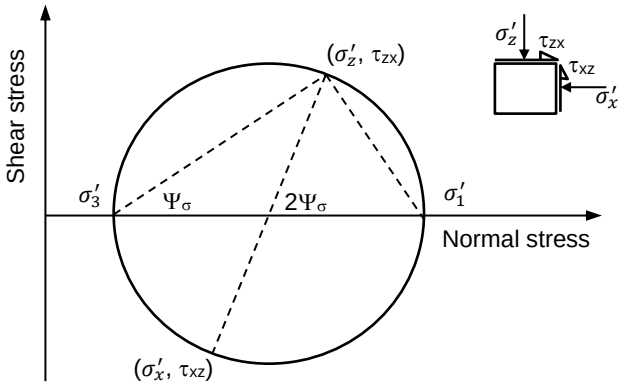

Figure 3. Estimation of stresses from DSS test results

Unfortunately, these two stresses are not sufficient to construct a Mohr's circle and determination of shear strength parameters. Several studies are available to address these issues. In the following sections, two approaches are discussed and compared with FE simulation results. Firstly, the estimation of principal stresses (σ_1' & σ_3') (Oda 1975), and secondly, the estimation of lateral stress (σ_x') (Frydman and Talesnick 1991).

4.1 Estimation of principal stresses

The rotation of principal stress direction with shearing in a simple shear test was examined in several studies, and the following relationship has been proposed (e.g., Ochiai et al. 1983; Oda and Konishi 1974; Oda 1975a, b).

$$R = k \tan\Psi_\sigma \quad (1)$$

$$k = \sin\phi_{cv}' \quad (2)$$

Where Ψ_σ is the inclination of the major principal stress to the vertical, ϕ_{cv}' is the angle of internal friction at constant volume (i.e., critical state), and k is a material property. The value of k is constant irrespective of applied normal stress, initial void ratio, stress path, and initial fabric (Cole 1967).

Several approaches have been proposed to estimate the value of the parameter k. Airey et al. (1985) and Borin (1973) suggested that k is slightly greater than $\tan\phi_{cv}'$. For Leighton Buzzard sand, Ochiai et al. (1983) and Oda (1975a) independently found that Eq. (2) could be used to estimate the value of k, based on the assumption that the principal axes of stress and strain increments coincide at the critical state (Cole 1967).

Ochiai et al. (1983) carried out a series of simple shear experiments and proposed the following empirical equation for Ψ_σ as a function of stress ratio R.

$$\Psi_\sigma = 1.82R - 0.75R^2 \text{ (in rad.)} \quad (3)$$

Now for a given R (known in DSS tests), the value Ψ_σ can be calculated using Eq. (3), which is then used to calculate $\tan\Psi_\sigma$ and plotted against R in Fig. 4. The slope of this R vs $\tan\Psi_\sigma$ line gives the value of k in Eq. (1). Figure 4 also shows the plot of R vs $\tan\Psi_\sigma$ (Eq. (1)) if $k = \sin\phi_{cv}'$ (i.e., Eq. (2) is used with ϕ_{cv}'= 32° (typical value of critical state friction angle). There is no significant difference between these two lines. In the following sections, $k = \sin\phi_{cv}'$ is used.

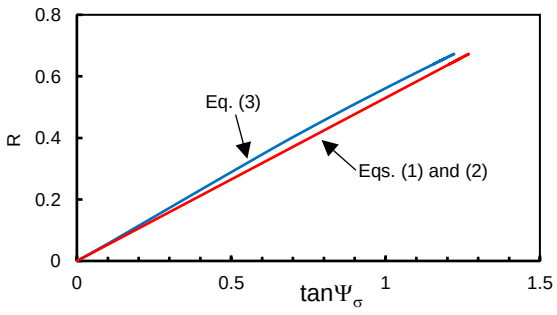

Figure 4. Variation of k with shear stress increase and rotation of principal stress

4.2 Estimation of lateral stress

Lateral stress is not measured in typical DSS tests. However, some modification was done in some studies to measure lateral stress (e.g., Budhu 1984, 1985; Kang and Kang 2015).

Frydman and Talesnick (1991) showed that the lateral stress (σ'_x) of a simple shear element can be estimated from the following equation.

$$\sigma'_x = [1 - k + R^2/k]\,\sigma'_z \quad (4)$$

The applicability of Eq. (4) is evaluated using the present FE simulation results. For each time increment, the vertical and lateral reaction forces acting on the rigid top plate is obtained from the simulation results. Dividing these forces by the cross-sectional area of the specimen (A), the normal (σ'_z) and shear (τ_{zx}) stresses acting on the plane for that shear strain level (γ) is obtained, which are then used to calculate R (= τ_{zx}/σ'_z). Now inserting R and k (= $\sin\phi'_{cv}$), the value of σ'_x is calculated using Eq. (4).

As will be shown in later sections, stress nonuniformity occurs mainly near the boundaries. Therefore, to compare with FE simulation results, the average of lateral stresses σ'_x for all the soil elements in a central core (6 mm thick and 36 mm diameter in the middle of the specimen) is calculated.

The empirical parameter in Eq. 4 has been derived from a wide range of laboratory tests (Ochiai et al. 1983). Fig. 5 shows the comparison of calculated lateral stress using Eq. (4) and average lateral stress in the soil elements in the central core. No significant difference is found between the calculated σ'_x, which implies that Eq. (4) could be used for a reasonable estimation of σ'_x.

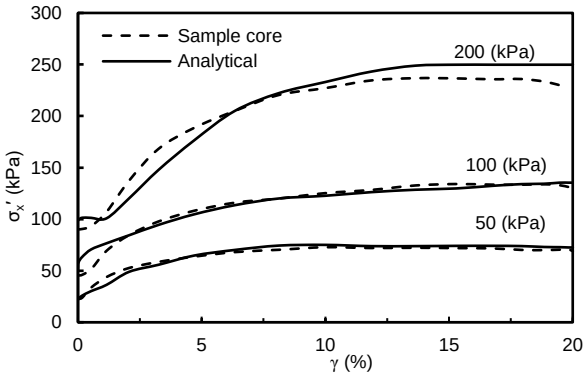

Figure 5. Estimation of lateral stress in DSS tests

4.3 Mobilized friction angle

The above discussion suggests that Mohr's circle could be constructed for the DSS test results by estimating principal stresses or lateral stress (Fig. 3). Now, using the values of σ'_z and τ_{zx} at the shear strain level of 15%, when the stress–strain curve becomes almost horizontal, and principal /lateral stresses, the Mohr's circle is contracted. Now drawing a tangent to this circle, the angle of internal friction is calculated for different normal stress levels. Table 2 shows that the calculated friction angle is lower (0.9°–3.2°) than the angle of internal friction given as the input parameter (38°), and the difference increases with an increase in normal stress. One potential reason behind this is the stress nonuniformity, which is discussed further in the following sections.

Table 2. Friction angle based on estimated values of non-measured stresses

	σ'_z = 50 kPa	σ'_z = 100 kPa	σ'_z = 200 kPa
Based on principal stresses	37.1°	35.9°	35.3°
Based on lateral stress	36.8°	35.6°	34.8°

5 STRESS NONUNIFORMITIES

Stress nonuniformity is one of the limitations of the DSS test. Nonuniformity occurs not only near the cylindrical vertical face (Wai et al. 2022; Wu 2017) but also near the top and bottom surfaces of the specimen (DeGroot et al. 1994; Wai et al. 2022; Wu 2017). The nonuniformity of stresses coupled with unknown normal and shear stresses on the cylindrical surface cause the interpretation of the test results to be challenging; for example, a Mohr's circle cannot be drawn as in the triaxial test. Several studies have assessed the degree of nonuniformity and its effects on the boundary stress (Asadzadeh and Soroush 2016; Bernhardt et al. 2016; DeGroot et al. 1994; Wai et al. 2022; Wijewickreme et al. 2013; Wu 2017). In the following sections, the nonuniformities of stresses are investigated using the simulation results for σ'_z = 100 kPa.

To show the variation of stresses, five paths are created (Fig. 6). Paths 1 and 2 are along the x-axis and 1.0-mm inside the soil from the top and bottom plates, respectively. Paths 4 and 5 are along the z-axis and again 1.0-mm inside the soil from the left and right vertical surfaces, respectively. Finally, path 3 is a circular line at a radial distance of 25-mm and 1.0-mm inside the soil from the top.

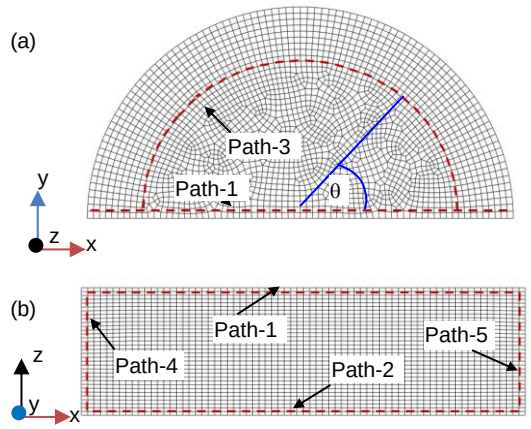

Figure 6. Paths to show stress distribution: (a) top view, (b) side view.

5.1 Distribution of shear stresses along the paths

Figure 7 shows that the distribution of shear stress (τ_{zx}) along the paths 1 and 2 is not uniform. The shear stress drops to a small value in the upper right and lower-left corners of the soil sample (see points c and a in the inset of Fig. 7). However, τ_{zx} in the middle two-thirds is almost uniform throughout the test. Modelling the soil as an elastic material, Roscoe (1953) also showed a similar pattern of shear stress distribution along the horizontal boundaries.

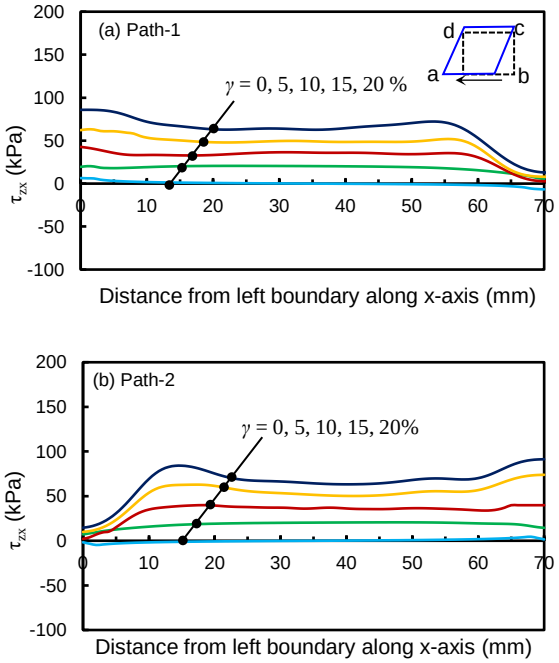

Figure 7. Distribution of shear stress for varying shear strains under σ'_z = 100 kPa: (a) along path-1 and (b) along path-2

The distribution of shear stress (τ_{xz}) along the Paths 4 and 5 is shown in Fig. 8. Shear stress concentration occurs at the top left and bottom right corners of the soil sample (near points d and b of the inset). Note that higher shear stress also generated in these corners, as shown in Fig. 7. However, τ_{xz} is relatively smaller in the other two corners. At the lower strain level (γ = 0–5%), the shear stress distribution along these paths is almost uniform. With increase in γ (e.g., γ = 15%) shear stress nonuniformity increases.

5.2 Distribution of vertical normal stresses

Figure 9 shows the vertical normal stress (σ'_z) distribution along path-1 and path-2. As no wall friction is considered at the vertical boundary, the normal stress distribution at the end of consolidation (i.e., beginning of the shearing, γ = 0) is uniform. With shearing, σ'_z becomes nonuniform, although the total force applied from the top plate is kept the same. σ'_z is considerably higher than 100 kPa within ~5 mm in the top left (point d in the inset) and bottom right corners (point b). On the other hand, σ'_z is considerably lower than 100 kPa in the soil elements near the top right and bottom left corners.

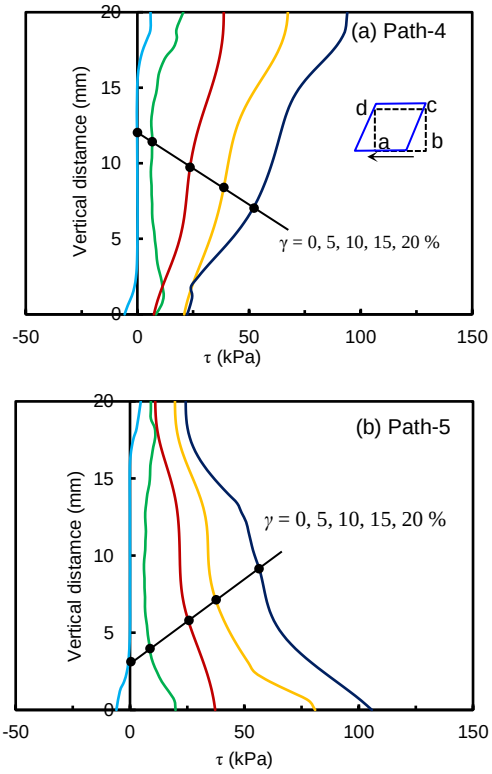

Figure 8. Distribution of shear stress for varying shear strain level under σ'_z = 100 kPa: (a) along path-4 and (b) along path-5

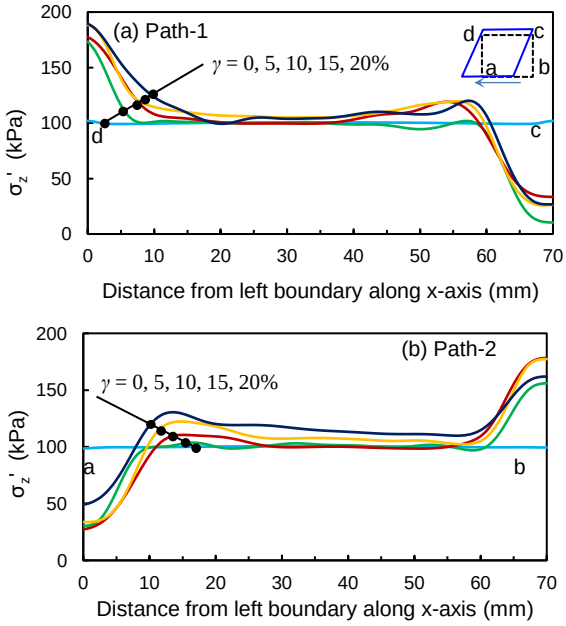

Figure 9. Distribution of vertical normal stress for varying shear strain level: (a) along path-1 and (b) along path-2

A similar trend has also been shown in previous studies (e.g., Budhu and Britto 1987; Finn 1978; Lucks et al. 1972; Wai et al. 2022; Wu 2017). However, Figs. 9(a) and 9 (b) show that the vertical stress remains almost constant at the targeted value (100 kPa) in the middle two-thirds of the specimen for the whole range of shear strain levels simulated in this study.

Figure 10 shows the vertical normal stress distribution along the radial path-3, as shown in Fig. 6. In this figure, the radial distance from the origin represents the σ_z' at a point on path 3 at angle θ to the horizontal (see Fig. 6). Again, σ_z' is uniform at the beginning of shearing (symmetric in Fig. 10). With increase in shear strain, stress nonuniformity develops (non-symmetric curves). The left half of the soil specimen experiences higher σ_z' than the right half for these soil elements near the top cap. An opposite pattern is found for the soil elements near the bottom pedestal.

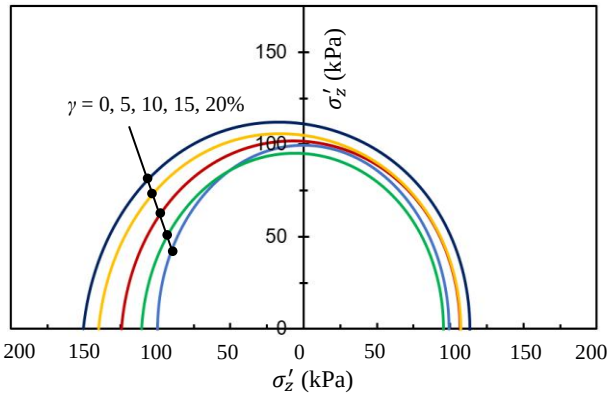

Figure 10. Distribution of vertical normal stress for varying shear strain levels along path-3

5.3 Plastic shear strains

Figure 11 shows the development of maximum plastic shear strain (ε_p^d) with loading. After a certain level of shearing, plastic shear strain accumulation occurs locally and failure planes form. To show the plastic shear strains and failure planes, the front view (left column of Fig. 11) and rare view (right column of Fig. 11) are shown. The plastic shear strain is small and almost homogeneous throughout the specimen during the early stage of shearing, especially in the central area. At γ = 2%–3%, a shear band (zone of large plastic shear strain) develops in the middle of the soil specimen. As the simulation progressed, this diagonal shear band extents towards the boundary and separates the specimen into two parts (Figs. 11(a) & 11(b)). A similar pattern of the rupture zone on the cylindrical soil sample is also reported by Budhu (1984) using the radiographic technique. In addition, considerably large plastic shear strains develop in the soil elements near the top and bottom plates could affect the stress distribution, such as lateral stress on the rings and stress nonuniformity.

6 DISCUSSION AND CONCLUSIONS

Direct simple shear test is one of the advanced methods of geotechnical testing as the test conditions are similar to many field conditions. However, stress nonuniformity and estimation of shear strength parameters (e.g., angle of internal friction) are some of the issues of DSS tests pointed out in several studies. Finite element analysis can provide some insights into the response, which can also explain the usefulness of the test results.

The present study simulates DSS tests on dry sand using a relatively simple elastic-plastic model. Comparing the FE simulation results, it is shown that the existing empirical relations could be used to estimate unknown lateral stress and principal stresses, which could be used to develop the Mohr's circle. The calculated angle of internal friction based on the developed Mohr's circle is slightly lower than the input value of the friction angle given for the Mohr–Coulomb model.

Nonuniformities developed near the boundaries, especially near the vertical surfaces because of the lack of complementary shear stress development at the soil–ring interface. Large plastic shear strains develop with shearing and shear bands form, which separates the soil specimens into blocks, especially at large shear strains. The formation of shear bands could affect stress development and nonuniformities at large strains.

Analyses presented in the paper do not consider the variation of density and strain-softening behaviour. Moreover, all the simulations are performed for constant normal stress conditions. Further studies are required, including the investigation of the above-mentioned issues.

7 ACKNOWLEDGEMENTS

The work presented in this paper has been supported by the Natural Sciences and Engineering Research Council of Canada (NSERC) and Equinor Research Chair grants.

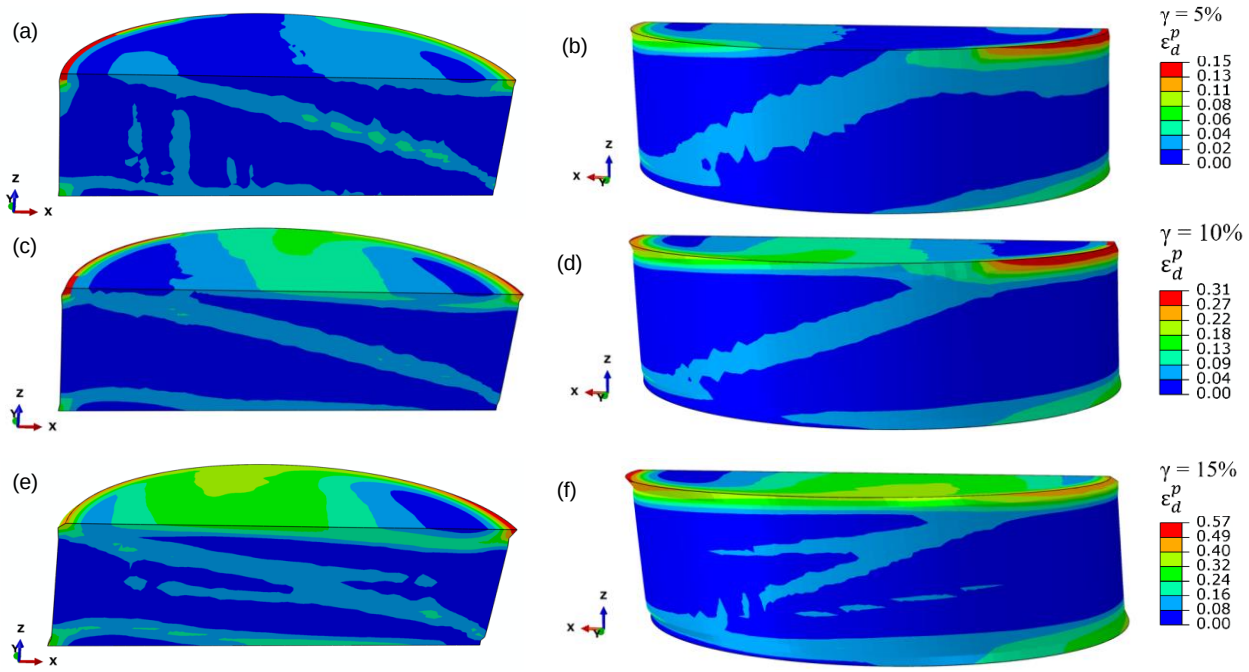

Figure 11. Maximum plastic strains for 100 kPa vertical normal stress: left colum front view and right column rare view

8 REFERENCES

ABAQUS (2019), "ABAQUS Documentation", Dassault Systèmes, RI, USA.

Asadzadeh, M. and Soroush, A., 2016. Fundamental investigation of constant stress simple shear test using DEM. *Powder Technology*, 292: 129-139.

Airey, D.W., Budhu, M. and Wood, D.M. 1985. 'Some aspects of the behaviour of soils in simple shear', in Banerjee, P.K. and Butterfield, R. (cds), Developments in Soil Mechanics and Foundation Engineering-2 Stress-Strain Modelling in Soils, Elsevier, Amsterdam: 185-213.

Al Tarhouni, M.A. and Hawlader, B. 2021. Monotonic and Cyclic Behaviour of Sand in Direct Simple Shear Test Conditions Considering Low Stresses, *Soil Dynamics and Earthquake Engineering*, 150: p.106931.

Bernhardt, M. L., Biscontin, G. and O'Sullivan, C. 2016. Experimental validation study of 3D direct simple shear DEM simulations, *Soils and Foundations*, 56(3): 336-347.

Borin, D.L. 1973. *The behaviour of saturated kaolin in the simple shear apparatus.* Ph.D. Thesis, University of Cambridge, Cambridge, England.

Budhu, M. 1984. Nonuniformities Imposed by Simple Shear Apparatus, *Canadian Geotechnical Journal*, 21(1): 125-137.

Budhu, M. 1985. Lateral Stresses Observed in Two Simple Shear Apparatus, *Journal of Geotechnical Engineering*, 111(6): 698-711.

Budhu, M. and Britto, A. 1987. Numerical Analysis of Soils in Simple Shear Devices, *Soils and Foundations*, 27(2): 31-41.

Budhu, M. 1988. Failure State of a Sand in Simple Shear, *Canadian Geotechnical Journal*, *25*(2): 395-400.

Cole, E.R.L. 1967. *The Behaviour of Soils in the Simple Shear Apparatus*. Ph. D. Thesis, University of Cambridge, Cambridge, England.

Dabeet, A., Wijewickreme, D. and Byrne, P. 2015. Evaluation of stress strain non-uniformities in the laboratory direct simple shear test specimens using 3D discrete element analysis, *Geomechanics and Geoengineering*, 10(4): 249-260.

DeGroot, D.J., Germaine, J.T. and Ladd, C.C. 1994. Effect of Nonuniform Stresses on Measured DSS Stress–Strain Behavior, *Journal of Geotechnical Engineering*, 120(5): 892-912.

Doherty, J. and Fahey, M. 2011. Three-Dimensional Finite Element Analysis of the Direct Simple Shear Test, *Computers and Geotechnics*, 38(7): 917-924.

Finn, W.D. 1985. Aspects of constant volume cyclic simple shear, In *Advances in the art of testing soils under cyclic conditions,* ASCE: 74-98.

Frydman, S. and Talesnick, M. 1991. Simple Shear of Isotropic Elasto-Plastic Soil, *International Journal for Numerical and Analytical Methods in Geomechanics*, 15(4) : 251-270.

Guo, J., Bernhardt-Barry, M.L. and Biscontin, G. Evaluation of Boundary Effects in Simple Shear Tests Using Discrete Element Modelling. In *Geo-Congress 2022*: 599-607.

Hardin, B.O., and Black, W.L. 1966. Sand stiffness under various triaxial stress. Journal of the Soil Mechanics and Foundations Division, ASCE, 92(SM2): 27–42.

Kang X, Kang G. (2015) Modified monotonic simple shear tests on silica sand. Journal of Marine Georesources & Geotechnology, 33: 122–126.

Lucks, A.S., Christian, J.T., Brandow, G.E. and Höeg, K. 1972. Stress Conditions in NGI Simple Shear Test, *Journal of the Soil Mechanics and Foundations Division*, 98(1): 155-160.

Ochiai, H., Yamanouchi, T. and Tanabashi, Y. 1983. On the Rotation of Principal Stress Axes in the Simple Shear Test and Its Utilizations, *Advances in the Mechanics and the Flow of Granular Materials*, 2: 871-883.

Oda, M. 1975 a. On the Relation $\tau/\sigma_N = \kappa \cdot \tan\psi$ in the Simple Shear Test, *Soils and Foundations*, 15(4): 35-41.

Oda, M. 1975 b. On Stress-dilatancy Relation of Sand in Simple Shear Test. *Soils and Foundations*, 15(2): 17-29.

Oda, M. and Konishi, J. 1974. Rotation of principal stresses in granular material during simple shear, *Soils and Foundations*, 14(4): 39-53.

Potts, D.M., Dounias, G.T. and Vaughan, P.R. 1987. Finite element analysis of the Direct Shear Box Test. *Géotechnique*, 37(1): 11-23.

Pradhan, T.B., Tatsuoka, F. and Horii, N. 1988. Simple shear testing on sand in a torsional shear apparatus, *Soils and Foundations*, *28*(2): 95-112.

Roscoe, K.H. 1953. An Apparatus for the Application of Simple Shear to Soil Samples. *In Proc. 3rd ICSMFE*, London, England, 1: 86-191.

Shibuya, S. and Hight, D. W. 1987. On the Stress Path in Simple Shear, *Géotechnique*, 37(4): 511–515.

Wai, D., Manmatharajan, M.V. and Ghafghazi, M. 2022. Effects of Imperfect Simple Shear Test Boundary Conditions on Monotonic and Cyclic Measurements in Sand, *Journal of Geotechnical and Geoenvironmental Engineering*, 148(1): p.04021164.

Wijewickreme, D., Dabeet, A. and Byrne, P. 2013. Some Observations on the State of Stress in the Direct Simple Shear Test Using 3D Discrete Element Analysis, *Geotechnical Testing Journal*, 36(2): 292-299.

Wu, Z. 2017. *Mechanical Modelling of Sand Considering Simple Shear Condition and Its Application to Pile Foundation.* Ph.D. Thesis, École centrale de Nantes.